

Spectroscopy and scattering matrices with nitrogen atom: Rydberg states and optical oscillator strengths

Yuhao Zhu(朱宇豪), Rui Jin(金锐), Yong Wu(吴勇), and Jianguo Wang(王建国)
Citation: Chin. Phys. B, 2022, 31 (**4**): 043103. DOI: 10.1088/1674-1056/ac1f05
Journal homepage: http://cpb.iphy.ac.cn; http://iopscience.iop.org/cpb

What follows is a list of articles you may be interested in

Transition parameters of Li-like ions (*Z*=7-11) in dense plasmas

Xiang-Fu Li(李向富), Li-Ping Jia(贾利平), Hong-Bin Wang(王宏斌), and Gang Jiang(蒋刚)
Chin. Phys. B, 2021, 30 (**5**): 053102. DOI: 10.1088/1674-1056/abea80

Dirac R-matrix calculations of photoionization cross sections of Ni XII and atomic structure data of Ni XIII

R T Nazir, M A Bari, M Bilal, S Sardar, M H Nasim, M Salahuddin
Chin. Phys. B, 2017, 26 (**2**): 023102. DOI: 10.1088/1674-1056/26/2/023102

Atomic structure and transition properties of H-like Al in hot and dense plasmas

Xiang-Fu Li(李向富), Gang Jiang(蒋刚), Hong-Bin Wang(王宏斌), Qian Sun(孙乾)
Chin. Phys. B, 2017, 26 (**1**): 013101. DOI: 10.1088/1674-1056/26/1/013101

Calculations of the dynamic dipole polarizabilities for the Li^+ ion

Yong-Hui Zhang(张永慧), Li-Yan Tang(唐丽艳), Xian-Zhou Zhang(张现周), Ting-Yun Shi(史庭云)
Chin. Phys. B, 2016, 25 (**10**): 103101. DOI: 10.1088/1674-1056/25/10/103101

Transition probabilities and lifetimes of the low-lying levels of Fe XIV

Fan Jian-Zhong, Wang Qing-Min, Chang Zhi-Wei, Dong Chen-Zhong
Chin. Phys. B, 2012, 21 (**6**): 063102. DOI: 10.1088/1674-1056/21/6/063102

Spectroscopy and scattering matrices with nitrogen atom: Rydberg states and optical oscillator strengths

Yuhao Zhu(朱宇豪)[1,†], Rui Jin(金锐)[2], Yong Wu(吴勇)[1,3,‡], and Jianguo Wang(王建国)[1]

[1] *Key Laboratory of Computational Physics, Institute of Applied Physics and Computational Mathematics, Beijing* 100088, *China*
[2] *Center for Free-Electron Laser Science, DESY, Hamburg* 22607, *Germany*
[3] *HEDPS, Center for Applied Physics and Technology, Peking University, Beijing* 100084, *China*

(Received 14 June 2021; revised manuscript received 15 August 2021; accepted manuscript online 19 August 2021)

The scattering matrices of $e + N^+$ with $J^\pi = 1.5^+$ in discrete energy regions are calculated using the eigenchannel R-matrix method. We obtain good parameters of multichannel quantum defect theory (MQDT) that vary smoothly as the function of the energy resulting from the analytical continuation property of the scattering matrices. By employing the MQDT, all discrete energy levels for N could be calculated accurately without missing anyone. The MQDT parameters (i.e., scattering matrices) can be calibrated with the available precise spectroscopy values. In this work, the optical oscillator strengths for the transition between the ground state and Rydberg series are obtained, which provide rich data for the diagnostic analysis of plasma.

Keywords: eigenchannel R-matrix, oscillator strengths

PACS: 31.15.ae, 31.15.ag **DOI:** 10.1088/1674-1056/ac1f05

1. Introduction

Atomic energy levels and optical oscillator strengths, particularly for Rydberg states, are crucial physical parameters in many physics fields, e.g., astrophysical spectroscopy,[1–3] diagnostic analysis of plasma,[4,5] quantum information processing[6–8] and so on. Specifically speaking, optical oscillator strengths between energy states are important for the understanding of energy balance and the rate of radiative decay in various types of astrophysical and laboratory plasma.[9–11] With the determination of line intensity ratios, the electron temperature, electron density and elemental abundances in plasma are indicated. In some special plasma environments, the radiation of Rydberg states cannot be neglected, e.g., the hot dense plasma.[12,13] Higher requirements are put forward for the richness of atomic energy levels and optical oscillator strengths. Although experimental measurements in spectroscopy have already made large promotion, they still cannot completely avoid absolute discrepancies. Therefore, precise theoretical calculations need play an indispensable role in atomic energy levels and optical oscillator strengths.

While traditional atomic structure calculation methods, such as the configuration interaction[14] (CI) method and many-body perturbation theory[15] (MBPT), are generally believed that the computational costs are too expensive for Rydberg states. Fortunately, there is a correlative relationship between the atomic energy levels and corresponding electron–ion collision processes in terms of the analytical continuation property of the short-range scattering matrices.[16–18] Depending on this property, the eigenchannel based on a relativistic R-matrix (R-R-Eigen)[19–21] could provide the required atomic data mentioned above with adequate precision. In the scenario of an R-R-Eigen, a half-collision model where it could be regarded as an ion in low-lying excited states combined with an incident electron in the bound orbital or the continuum orbital composes the atomic system. Whatever in the bound or continuum energy regions, the short-range scattering matrices for the multi-channel process can be calculated accurately. One can extract the needed physical parameters in multi-channel quantum defect theory (MQDT)[22–26] from the scattering matrices, i.e., the eigenchannel phase and transformation matrix. Due to the analytical continuation of the scattering matrices, MQDT parameters vary smoothly as a function of energy. It is sufficient for us to calculate the scattering matrices with a minority of energy points in order to obtain good MQDT parameters for the entire energy of interest. By employing the MQDT, all energy level positions in discrete energy regions will be predicted without missing anyone. Furthermore, various electron dynamics processes in atomic systems can be calculated using MQDT parameters (i.e., scattering matrices) checked by precise spectroscopy measurements, such as those of scatter, optical absorption, and radiation.

Nitrogen is one of the most abundant elements found both on Earth and in the atmospheres of stars with huge demand for spectral line diagnosis. As an open-shell element, nitrogen also is extremely useful for plasma modeling. Previous research works[27–33] on the nitrogen atom have mainly studied the electronic structures and transitions for low-lying energy states because of the correlation effect of electrons. How-

†Corresponding author. E-mail: zhu_yuhao@foxmail.com
‡Corresponding author. E-mail: wu_yong@iapcm.ac.cn

© 2022 Chinese Physical Society and IOP Publishing Ltd

ever, we are able to stretch the energy region to the extent of high Rydberg states with high precision and less computational costs using R-R-Eigen. In this work, the nitrogen atom has been investigated for the specific partial wave $J^{\pi} = 1.5^{+}$ (+ represents even parity). The present paper is organized as follows. The MQDT parameters of the selected physical channels are obtained in Subsection 2.1. The discrete energy levels of the major Rydberg series are calculated in Subsection 2.2. In Subsection 2.3, we calculate the optical oscillator strengths for the transition between the ground state and parts of the Rydberg series. The partial theoretical energy levels and corresponding optical oscillator strengths are exhibited in detail. Finally, the paper ends with a short summary.

Table 1. Physical channels with corresponding eigenchannels for N system with $J^{\pi} = 1.5^{+}$ symmetry.

Index	1	2	3	4	5	6
Physical channels	$^3P_1s_{1/2}$	$^3P_2s_{1/2}$	$^3P_0d_{3/2}$	$^3P_1d_{3/2}$	$^3P_1d_{5/2}$	$^3P_2d_{3/2}$
Eigenchannels	$^4P_{3/2}$	$^2P_{3/2}$	$^4F_{3/2}$	$^4D_{3/2}$	$^2D_{3/2}$	$^4P_{3/2}$
Index	7	8	9	10	11	12
Physical channels	$^3P_2d_{5/2}$	$^3P_2g_{7/2}$	$^1D_2s_{1/2}$	$^1D_2d_{3/2}$	$^1D_2d_{5/2}$	$^1D_2g_{7/2}$
Eigenchannels	$^2P_{3/2}$	$^4F_{3/2}$	$^2D_{3/2}$	$^2D_{3/2}$	$^2P_{3/2}$	$^2D_{3/2}$

2. Theoretical methods and calculation results

2.1. Calculation of the MQDT parameters

The construction of the nitrogen atom system is from the model of an electron collision with a nitrogen cation. The wavefunction of the N + 1 system (i.e., ion with an electron) is solved by a method that seems like a traditional relativistic R-matrix.[34–37] In the inner region, the scattering system is treated as the bound state, i.e., the CI expansion of the internal wavefunction, since there is a strong exchange and correlation effects between the scattering electron and the target electrons. On the other hand, the incident electron is in the long-range multipole potential field of the target in the outer region. We can obtain the exact wavefunction of the electrons by neglecting the exchange and correlation effects. The inner and outer wavefunctions are connected by the R matrix to construct the total wavefunction of the N + 1 system. Thus, we can derive the reaction matrices (K matrices) from the N + 1 electron wavefunction defined on a certain boundary in the reaction zone. The electron wavefunction in the R-R-Eigen is as follows:

$$\psi_i(E) = \varphi_i f_i(r_{\mathrm{N}+1}, E) + \sum_{j=1}^{n_{\mathrm{p}}} \varphi_j \mathrm{g}_j(r_{\mathrm{N}+1}, E) K_{ij} + \sum_{j=n_{\mathrm{p}}+1}^{n_{\mathrm{p}}+n_{\mathrm{c}}} \varphi_j \Theta_j(r_0, E), \quad i \le n_{\mathrm{p}}, \tag{1}$$

where n_{p} and n_{c} are the number of physical and computational channels, and Θ_j is the corresponding radial wavefunctions of the N + 1 electron system. Note that the definitions of the channels are different from the traditional R-matrix.[38] For the i^{th} physical channel, the regular and irregular Coulomb wavefunctions, $f_i(r_{\mathrm{N}+1}, E)$ and $\mathrm{g}_j(r_{\mathrm{N}+1}, E)$, modified by the appropriate long-range polarization interactions, cover the entire set of the one-electron orbitals, with both negative and positive energy.[23] The scattering matrices S_{ij} are extracted from the reaction matrices K_{ij}. We transform the wavefunction into an eigenchannel representation and the short-range scatter matrices with a specific total angular momentum and parity J^{π} are diagonalized as follows:

$$S_{ij} = \sum_{\alpha} U_{i\alpha} \exp(\mathrm{i}2\pi\mu_{\alpha}) U_{j\alpha}, \tag{2}$$

where the eigenchannel phase μ_{α} and $n_{\mathrm{p}} \times n_{\mathrm{p}}$ orthogonal transformation matrix $U_{i\alpha}$ are the main parameters in MQDT. The transformation matrix between the eigenchannels and physical channels $U_{i\alpha}$ can usually be characterized as Euler-type angles[16,22] θ_k, $k = 1, \ldots, n_{\mathrm{p}}(n_{\mathrm{p}} - 1)/2$.

We take account of 12 physical channels in the scattering matrices calculation of N with $J^{\pi} = 1.5^{+}$ symmetry. As the scattering energy varies from the bound-state energy region to the continuum-state energy region, the number of physical channels increases gradually rises from the mathematical properties of the Coulomb wavefunctions,[39] i.e., 2, 5, 8, and 12 channels are in the four different energy regions, respectively. More specifically, in the energy region of −0.225 Ry to −0.125 Ry, there are two physical channels, namely, $\mathrm{N}^+(^3\mathrm{P}_1)\mathrm{s}_{1/2}$ and $\mathrm{N}^+(^3\mathrm{P}_2)\mathrm{s}_{1/2}$. In the energy of −0.125 Ry to −0.06 Ry, there are five physical channels with three additional channels, namely, $\mathrm{N}^+(^3\mathrm{P}_0)\mathrm{d}_{3/2}$, $\mathrm{N}^+(^3\mathrm{P}_1)\mathrm{d}_{3/2}$, $\mathrm{N}^+(^3\mathrm{P}_1)\mathrm{d}_{5/2}$. Three extra channels in the eight physical channels energy region of −0.06 Ry to 0.08 Ry are $\mathrm{N}^+(^3\mathrm{P}_2)\mathrm{d}_{3/2}$, $\mathrm{N}^+(^3\mathrm{P}_2)\mathrm{d}_{5/2}$, $\mathrm{N}^+(^3\mathrm{P}_2)\mathrm{g}_{7/2}$, respectively. The 12 physical channels with four additional channels, i.e., $\mathrm{N}^+(^1\mathrm{D}_2)\mathrm{s}_{1/2}$, $\mathrm{N}^+(^1\mathrm{D}_2)\mathrm{d}_{3/2}$, $\mathrm{N}^+(^1\mathrm{D}_2)\mathrm{d}_{5/2}$, $\mathrm{N}^+(^1\mathrm{D}_2)\mathrm{g}_{7/2}$, are in the final energy region of 0.08 Ry to 0.18 Ry. For better identification of physical channels, we list all 12 physical channels (*JJ* notation) with their corresponding eigenchannels (*LS* notation) in Table 1. Due to the number of physical channels equal to the eigenchannels in each independent energy region, there are four transformation matrices $U_{i\alpha}$ with the same dimension as the number of eigenchannels, which are represented by 1, 10, 28, 66 Euler-type angles in the four energy regions respectively.

The MQDT parameters $U_{i\alpha}$ and μ_{α} varying via the energy are shown in Fig. 1(a) and 1(b), respectively. As we see, the MQDT parameters μ_{α} and $U_{i\alpha}$ vary as functions of the energy smoothly over the whole energy region, which substantially reflects the analytical continuation property of the scattering matrices. Evidently, all of the connections between the identical channels in the adjacent energy regions belong to the type-I

connection with weak interchannel interactions.[20] Based on the analytical continuation property of scattering matrices, all discrete energy levels can be obtained without missing anyone in the framework of the MQDT in the next section.

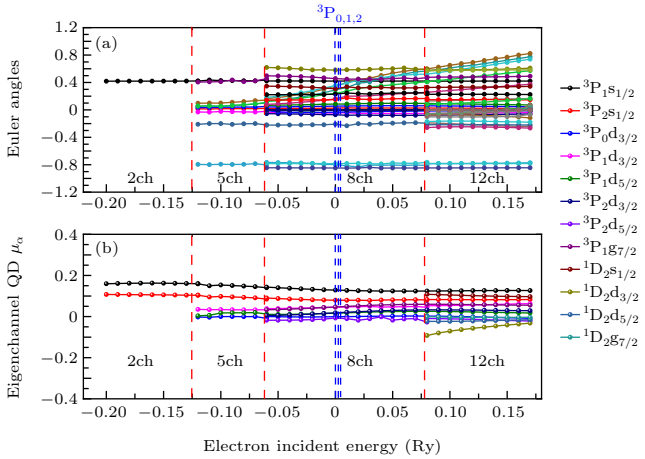


Fig. 1. Eigen-quantum defects μ_α, Euler angles θ_k for $U_{i\alpha}$ matrix in the $J^\pi = 1.5^+$ symmetry of N. The dashed red lines indicate the connection position of different channel regions. The zero energy of abscissa represents the first ionization threshold of $^3P_0$ and all the ionization thresholds of N are plotted with the dashed blue lines. Note that the labels of channels on the right are only for eigen-quantum defects μ_α.

2.2. Calculation of the discrete energy levels

In order to obtain the discrete energy levels, we briefly introduce the MQDT. The energy eigenfunctions are expressed as the linear combination of eigenchannel wavefunctions, i.e.,

$$\Psi^{J^\pi} = \sum_\alpha A_\alpha \psi_\alpha^{J^\pi}(E), \tag{3}$$

where the A_α is the mixing coefficient and determined by the asymptotic boundary conditions. For the discrete spectrum, all the channels are closed and the boundary conditions require that energy eigenfunctions are zero at infinity leading to the following set of equations:

$$\sum_\alpha F_{i\alpha} A_\alpha = 0, \quad \text{for all } i, \tag{4}$$

$$F_{i\alpha} = U_{i\alpha} \sin \pi(\nu_i + \mu_\alpha), \tag{5}$$

with the effective principal quantum numbers ν_i defined as

$$E = I_i - q^2/\nu_i^2 \quad (\text{in Ry}), \tag{6}$$

where I_i is the ionization threshold and q is the charge of the target ion. The system of linear Eq. (4) has the following compatibility condition:

$$F(\{\nu_i\}) = \det[U_{i\alpha} \sin \pi(\nu_i + \mu_\alpha)] = 0, \tag{7}$$

and the nontrival solutions

$$A_\alpha = C_{i\alpha} / \left(\sum_\alpha C_{i\alpha}^2 \right)^{1/2}, \tag{8}$$

where $C_{i\alpha}$ is the cofactor of the element $F_{i\alpha}$ of the determinant $|F_{i\alpha}|$, and the choice of index i is arbitrary. The solutions to Eqs. (5) and (6), i.e., discrete sets of the numbers ν_i, provide discrete energy levels of the perturbed Rydberg series.

Utilizing the smooth MQDT parameters, we can solve Eqs. (5) and (6) to obtain the energy levels that can be compared with the precision spectroscopic measurements to correct scattering matrices. In our case of the nitrogen atom with $J^\pi = 1.5^+$, three thresholds are involved in the interested energy region leading to three principal quantum numbers $\nu_{^3P_0}, \nu_{^3P_1}, \nu_{^3P_2}$. For the atomic system with more than two ionization thresholds, one can adopt a projected high dimensional quantum-defect graph (symmetrized), i.e., JHANGZ plot, to show the results of the graphic method. More precisely, we use the energy constraint from Eq. (5) to project the problem of three-dimensional solution of Eq. (6) (i.e., three unknown variables) to an advisable two-dimensional subspace through selecting arbitrary two of the three principal quantum numbers $(\nu_{^3P_0}, \nu_{^3P_1}, \nu_{^3P_2})$ as known variables. In this calculation, it is appropriate to select a two-dimensional plot with $\nu_{^3P_0}$ versus $-\nu_{^3P_1}$ as a way of physical understanding. Thus, the $\nu_{^3P_1}$ is the known variables with unknown variables $\nu_{^3P_0}, \nu_{^3P_2}$ to scan the energy of $\nu_{^3P_1}$. Effective principal quantum numbers are projected out in Eq. (6) with the following energy constraint:

$$\begin{aligned} \Delta &= \nu_{^3P_2} - \nu_{^3P_0} \\ &= \left[1/\nu_{^3P_1} - (I_{^3P_1} - I_{^3P_2})/q^2\right]^{-1/2} \\ &\quad - \left[1/\nu_{^3P_1} - (I_{^3P_1} - I_{^3P_0})/q^2\right]^{-1/2}, \end{aligned} \tag{9}$$

where q is the target charge and I is the ionization threshold.

In Fig. 2 (JHANGZ plot), one can see that the seven differently colored branch curves determined by mixing coefficient A_α of the eigenchannel wavefunction represent the different eigenchannel effective phase shifts solved by Eq. (6). There are four quasi-horizontal differently colored branch curves, including black, red, orange and purple, which represent channels with $^3P_0d_{3/2}(^4F)$, $^3P_1s_{1/2}(^4P)$, $^3P_2d_{3/2}(^4P)$, $^3P_2d_{5/2}(^2P)$, respectively. On the other hand, three quasiperiodic resonant colored branch curves, blue, pink and green, represent channels with $^3P_1d_{3/2}(^4D)$, $^3P_1d_{5/2}(^2D)$, $^3P_2s_{1/2}(^2P)$, respectively. The dashed lines are the Rydberg relationship between the projected ionization thresholds $^3P_0$ and $^3P_1$. What is more, the crossing points between the dashed lines of the Rydberg relationship and solid curves of the seven colored branch curves are the theoretical energy level positions for the relevant eigenchannel. We have labeled the theoretical energy levels with various symbols, i.e., black circle, red triangle, blue five-pointed star, pink pentagon, green square, orange inverted triangle and purple rhombus, representing each eigenchannel determined by the corresponding color, respectively. The abscissa is the principal quantum number identified by Eq. (5) for the different eigenchannel. It is noted that discrepancies of

tunnel depth in the multi-electronic system result in diverse ν of s wave and d wave channels (decided by the different types of the incident continuous electron). For the condition of N with $J^{\pi} = 1.5^{+}$ symmetry, the 65 experimental values in the NIST[40] and corresponding existing theoretical values under these projection thresholds are labeled in Fig. 2. Compared with available experimental data, the precision of the short-range scattering matrices is estimated to be within 2%. In this framework, one can systematically obtain all energy levels without missing anyone by employing the MQDT, rather than calculating energy levels one by one like in traditional methods.

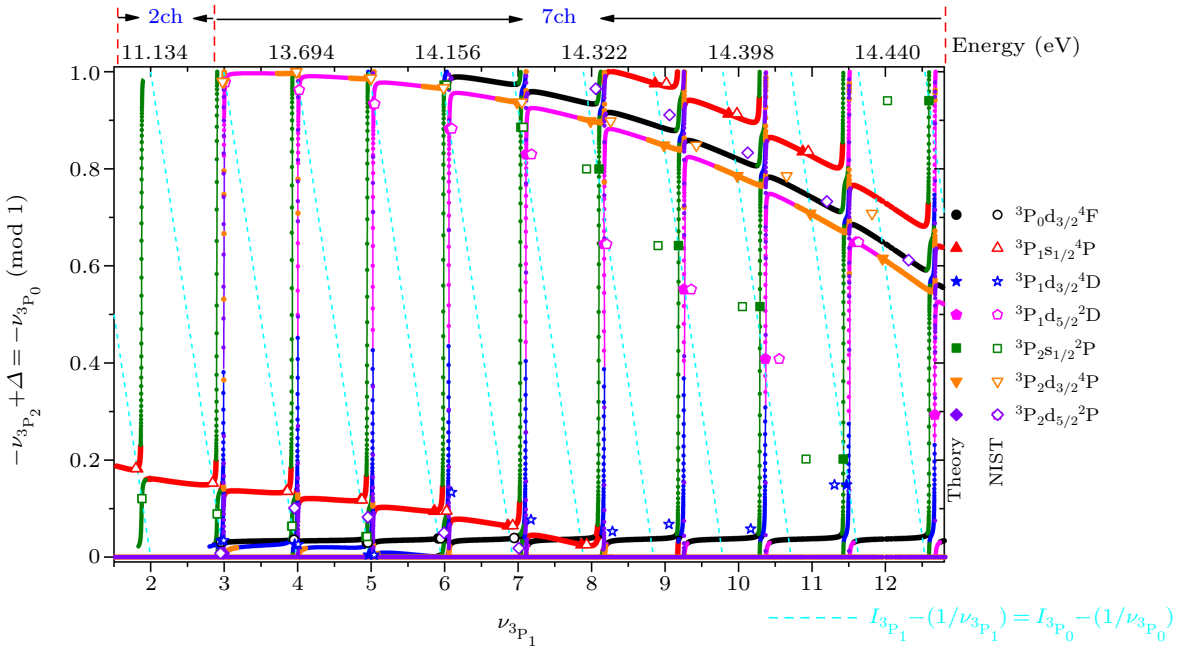


Fig. 2. Projected high-dimensional quantum-defect graph. Quantum-defect $-\nu_{^3P_0}$ (mod 1) versus $\nu_{^3P_1}$ plot of N $J^{\pi} = 1.5^{+}$ partial wave. The dashed cyan lines are the Rydberg relationship between the two ionizations of $^3P_0$ and $^3P_1$. The differently colored solid curves indicate $F = 0$, i.e., Eq. (6). The crossing points between the solid curves and dashed lines are the positions of theoretical energy levels. The corresponding energy level positions are labeled with different types of symbols. i.e., black circles are d wave ^4F, red triangles are s wave ^4P, blue five-pointed stars are d wave ^4D, pink pentagons are d wave ^2D, green squares are s wave ^2P, orange inverted triangles are d wave ^4P and purple rhombuses are d wave ^2P. All theoretical energies results are indicated as solid symbols, and available experimental energies are presented by the open symbols for comparison. Note that the energy grid at the top is not equidistant, but increasingly dense.

2.3. Optical oscillator strengths

After obtaining the exact eigenchannel wavefunction, optical absorption and radiation of atomic systems can be investigated. The optical oscillator strengths (OOSs) of n-th state could be derived from the mixing coefficient for the different channel via

$$f_n = \frac{2(E_n - E_0)\left[\sum_\alpha D_\alpha A_\alpha^{(n)}\right]^2}{N_n^2}, \tag{10}$$

where E_0 and E_n represent initial state energy and final state energy, D_α is the reduced dipole matrix element, which can be calculated using R-R-Eigen procedure,[19] and $A_\alpha^{(n)}$ is the mix coefficients of eigenchannel. N_n^2 is the normalization factor that can be expressed as[22,24]

$$N_n^2 = N_{0,n} \times \left[\nu_{0,n}^3 + \frac{N_{1,n}}{N_{0,n}}\nu_{1,n}^3 + \sum_\alpha \frac{\mathrm{d}\mu_\alpha}{\mathrm{d}E}(A_\alpha^{(n)})^2 + \sum_i \sum_\alpha \sum_\beta \frac{\mathrm{d}\mu_{i\alpha}}{\mathrm{d}E}\mu_{i\beta}\sin\pi(\mu_\alpha - \mu_\beta)A_\alpha^{(n)}A_\beta^{(n)}\right]. \tag{11}$$

We calculate the OOS of N for the transition between the ground state and a portion of the Rydberg series which have the same LS notation. It is noted that computational costs of the energy levels and OOSs for highly excited states are considerably less than for conventional methods.[14,15] In Table 2, the calculation results are listed, including the principal quantum number of the projected ionization threshold $\nu_{^3P_1}$, theoretical energy levels, experiments energy levels from NIST[40] and the length and velocity values of the oscillator strengths for the transition between the ground state $^4S^o_{3/2}$ and Rydberg series with the terms $^4P_{3/2}$ and $^2P_{3/2}$. The theoretical energy levels generally coincide with the experiments with a precision of better than one percent. To our knowledge, we only found calculations[27,28,31] that reported OOS for relevant fine structures with the configurations $2s^22p^23s$ and $2s^22p^23d$ in the transition conditions of $^4S^o_{3/2}$–$^4P_{3/2}$ and $^4S^o_{3/2}$–$^2P_{3/2}$. As we see, the discrepancies between our theoretical results and others[28,31] in the condition of configuration $2s^22p^23s$ with transition of $^4S^o_{3/2}$–$^4P_{3/2}$ are within 10%. However, the conditions of the configurations $2s^22p^23s$ and $2s^22p^23d$ with transition of $^4S^o_{3/2}$–$^2P_{3/2}$ are more than 10%, which may result from the different expansions of wavefunctions. Precisely, the basis

sets in our method are a group of scattering channel wavefunctions, others[28,31] have usually employed the traditional atomic orbital basis sets. We also found that there are few experimental and other theoretical results in highly excited states for comparison. As a matter of fact, it is an enormous challenge for experiments and traditional methods to study the optical oscillator strengths of the Rydberg states near the ionization threshold. Further experimental and theoretical studies on the OOSs of Rydberg states are necessary. As for the scenario of R-R-Eigen, a specific $N+1$ system channel can be ascertained in advance based on the principle of scattering. We can accurately obtain a series of bound states of this channel and corresponding dynamics conveniently through energy determination. Namely, the complete basis of the total electronic wavefunction is formed by the wavefunctions of different scattering channels.

Table 2. Energy levels and the length (L) and velocity (V) values of OOS for the transitions of $^4S^o_{3/2}$–$^4P_{3/2}$ and $^4S^o_{3/2}$–$^2P_{3/2}$ are listed. The $\nu_{^3P_1}$ is the principal quantum number for the state of corresponding Rydberg series.

Transition		Levels		OOS		Other theory	
$^4S^o_{3/2}$–$^4P_{3/2}$	$\nu_{^3P_1}$	Theory (eV)	NIST (eV)	L	V	L	V
$2s^22p^23s$	1.8000	10.3366	10.3301	1.067(−1)	1.032(−1)	1.02(−1)[a]	1.02(−1)[a]
$2s^22p^24s$	2.8429	12.8512	12.8531	0.332(−1)	0.332(−1)		
$2s^22p^25s$	3.8516	13.6173	13.6204	0.137(−1)	0.137(−1)		
$2s^22p^26s$	4.8572	13.9576	13.9618	0.657(−2)	0.629(−2)		
$2s^22p^27s$	5.8600	14.1480	14.1598	0.348(−2)	0.330(−2)		
$2s^22p^28s$	6.8618	14.2452	14.2506	0.200(−2)	0.189(−2)		
$2s^22p^29s$	7.8643	14.3142	14.3180	0.120(−2)	0.113(−2)		
$2s^22p^210s$	8.8652	14.3610	14.3669	0.784(−3)	0.739(−3)		
$2s^22p^211s$	9.8666	14.3944	14.3975	0.527(−3)	0.497(−3)		
$2s^22p^212s$	10.8673	14.4190	14.4208	0.362(−3)	0.342(−3)		
Transition		Levels		OOS		Other theory	
$^4S^o_{3/2}$–$^2P_{3/2}$	$\nu_{^3P_1}$	Theory (eV)	NIST (eV)	L	V	L	V
$2s^22p^23s$	1.8814	10.6911	10.6900	0.418(−5)	0.397(−5)	0.852(−5)[b]	1.171(−5)[b]
$2s^22p^24s$	2.9052	12.9228	12.9218	0.160(−3)	0.151(−3)		
$2s^22p^25s$	3.9207	13.6494	13.6511	0.526(−3)	0.485(−3)		
$2s^22p^26s$	4.9317	13.9749	13.9776	0.892(−3)	0.790(−3)		
$2s^22p^27s$	5.9935	14.1555	14.1598	0.440(−3)	0.360(−3)		
$2s^22p^28s$	7.0368	14.2594	14.2623	0.114(−3)	0.110(−3)		
$2s^22p^29s$	8.1007	14.3268	14.3180	0.104(−3)	0.986(−4)		
$2s^22p^210s$	9.1845	14.3729	14.3626	0.106(−3)	0.100(−3)		
$2s^22p^211s$	10.2925	14.4057	14.3954	0.875(−4)	0.822(−4)		
$2s^22p^212s$	11.4257	14.4299	14.4200	0.967(−4)	0.902(−4)		
$2s^22p^213s$	12.5926	14.4483	14.4401	0.734(−4)	0.688(−4)		
Transition		Levels		OOS		Other theory	
$^4S^o_{3/2}$–$^4P_{3/2}$	$\nu_{^3P_1}$	Theory (eV)	NIST (eV)	L	V	L	V
$2s^22p^23d$	2.9997	13.0198	13.0010	1.214(−2)	1.046(−2)	2.03(−2)[b]	2.10(−2)[b]
$2s^22p^24d$	3.9834	13.6771	13.6783	2.146(−2)	1.842(−2)		
$2s^22p^25d$	4.9846	13.9867	13.9901	8.623(−3)	7.408(−3)		
$2s^22p^26d$	5.9850	14.1544	14.1590	3.939(−3)	3.361(−3)		
$2s^22p^27d$	6.9856	14.2554	14.2605	2.502(−3)	2.146(−3)		
$2s^22p^28d$	7.9863	14.3209	14.3348	1.599(−3)	1.373(−3)		
$2s^22p^29d$	8.9865	14.3657	14.3810	1.089(−3)	9.347(−4)		
$2s^22p^210d$	9.9846	14.3977	14.4143	7.789(−4)	6.690(−4)		
$2s^22p^211d$	10.9862	14.4212	14.4368	5.759(−4)	4.947(−4)		
$2s^22p^212d$	11.9865	14.4390	14.4542	4.378(−4)	3.761(−4)		

[a]Tayal *et al.* (2006)[31], [b]Hibbert *et al.* (1985)[28].

3. Summary

With employing the R-R-Eigen method, we calculate the short-range scattering matrices of the $e+N^+$ system for $J^\pi = 1.5^+$ symmetry which provided good MQDT parameters $(\mu_\alpha, U_{i\alpha})$ in the energy region from −0.225 Ry to 0.18 Ry. The smoothness of the MQDT parameters (i.e., the analytical continuation of scattering matrices) is guaranteed by selecting the appropriate physical channels in different energy regions. Additionally, the accuracy of our calculated MQDT parameters is determined to be within 2%. All the connections of

the MQDT parameters in different energy regions belong to the type-I connection, which has weaker eigenchannels interactions compared with the type-II connection.[20] In the condition for multi-thresholds of the atomic system, we propose the JHANGZ plot to perform the final result of solving the MQDT equations in the discrete energy region. The JHANGZ plot shows theoretical energy level positions and experimental values for each channel systematically. The theoretical energy levels in the current work are within one percent discrepancy compared to the values of the NIST. According to the precise spectroscopy measurements, we could review the MQDT parameters to obtain more accurate results. Namely, given the analytical continuation property of scattering matrices, the smoothness of MQDT parameters in all energy regions is necessary. Thus, in order to ensure the smoothness of the MQDT parameters, the slope of the MQDT parameters varying with energy will not be distorted, only a small translation of the parameters as a whole. In this way, we shall improve the numerical accuracy of the results without destroying the analytical continuation property of scattering matrices.

In our work, the relevant physical channels dipole matrix elements D_α and the mixing coefficient of the eigenchannel wavefunction are calculated to obtain the optical oscillator strengths. The optical oscillator strengths for the transitions between the ground state and Rydberg series with terms $^4P_{3/2}$ and $^2P_{3/2}$ are exhibited thoroughly. There is good agreement between other theoretical calculations and ours in the condition of the configurations $2s^22p^23s$ and $2s^22p^23d$. The optical oscillator strengths could supply abundant information about the optical transition of highly excited states to help us understand the influence of the radiation on the energy balance of high energy levels in hot dense plasma. Moreover, we look forward to more experiments and theoretical calculations in further studies on the optical oscillator strengths of the Rydberg states.

Acknowledgments

Project supported by the Science Challenge Project (Grant No. TZ2016005), the National Key Research and Development Program of China (Grant Nos. 2017YFA0403200 and 2017YFA0402300), and the CAEP Foundation (Grant No. CX2019022). We thank the Institute of Applied Physics and Computational Mathematics for the supercomputing source.

References

[1] Dalgarno A 1979 *Advances in Atomic and Molecular Physics* **15** 37
[2] Kallman T R and Palmeri P 2007 *Rev. Mod. Phys.* **79** 79
[3] Beiersdorfer and Peter 2003 *Annual Review of Astronomy and Astrophysics* **41** 343
[4] Liu P F, Liu Y P, Zeng J L and Yuan J M 2014 *Phys. Rev. A* **89** 042704
[5] Lindl J D, Amendt P, Berger R L, Glendinning S G, Glenzer S H, Haan S W, Kauffman R L, Landen O L and Suter L J 2004 *Phys. Plasmas* **11** 339
[6] Saffman M, Walker T G and Mølmer K 2010 *Rev. Mod. Phys.* **82** 2313
[7] Petrosyan D and Nikolopoulos G M 2014 *Phys. Rev. A* **89** 013419
[8] Gallaghar T 1994 *Rydberg Atoms* (Cambridge: Cambridge University Press)
[9] Ralchenko Y, Chung H K, Scott H A and Hansen S B Jr 2016 *Modern Methods in Collisional-Radiative Modeling of Plasmas* (Springer International Publishing)
[10] Pierrot L, Yu L, Gessman R, Laux C and Kruger C 1999 *Collisional-radiative modeling of nonequilibrium effects in nitrogen plasmas 30th Plasmadynamic and Lasers Conference* p. 3478
[11] Bae L J, Zastrau U, Chung H K, Bernstein A C and Cho B I 2018 *Opt. Express* **26** 6294
[12] Bar-Shalom A, Oreg J, Goldstein W H, Shvarts D and Zigler A 1989 *Phys. Rev. A* **40** 3183
[13] Chung H K, Cho B I, Ciricosta O, Vinko S M, Wark J S and Lee R W 2017 *AIP Conference Proceedings* **1811** 020001
[14] Shavitt and Isaiah 1998 *Molecular Physics* **94** 3
[15] Lindgren I 1974 *J. Phys. B: Atom. Mol. Phys.* **7** 2441
[16] Gao X and Li J M 2014 *Phys. Rev. A* **89** 022710
[17] Gao X, Jin R, Zeng D L, Han X Y, Yan J and Li J M 2015 *Phys. Rev. A* **92** 052712
[18] Xiang G and Jia-Ming L 2012 *Chin. Phys. Lett.* **29** 89
[19] Jin R, Han X Y, Gao X, Zeng D L and Li J M 2017 *Scientific Reports* **7** 11589
[20] Zeng D L, Jin R, Gu C, Yue X F, Gao X and Li J M 2017 *Phys. Rev. A* **95** 042508
[21] Dou L J, Jin R, Sun R, Xie L Y, Huang Z K, Li J M, Ma X W and Gao X 2020 *Phys. Rev. A* **101** 032508
[22] Lee C M and Lu K T 1973 *Phys. Rev. A* **8** 1241
[23] Aymar M, Greene C H and Luc-Koenig E 1996 *Rev. Mod. Phys.* **68** 1015
[24] Lee C M and Johnson W R 1980 *Phys. Rev. A* **22** 979
[25] Lee C M 1974 *Phys. Rev. A* **10** 584
[26] Lee C M 1974 *Phys. Rev. A* **10** 1598
[27] Bell K and Berrington K 1991 *J. Phys. B: Atom. Mol. Opt. Phys.* **24** 933
[28] Hibbert A, Dufton P and Keenan F 1985 *Monthly Notices of the Royal Astronomical Society* **213** 721
[29] Robinson D and Hibbert A 1997 *J. Phys. B: Atom. Mol. Opt. Phys.* **30** 4813
[30] Tayal S S and Beatty C A 1999 *Phys. Rev. A* **59** 3622
[31] Tayal S 2006 *The Astrophysical Journal Supplement Series* **163** 207
[32] Bi P, Liu Y Q, Tang Y J, Yang X D and Lei H L 2010 *Acta Phys. Sin.* 59 (in Chinese)
[33] Yu X M, Qi C H and Wang C L 2018 *Chin. Phys. B* **27** 060101
[34] Burke P G 2011 *R-matrix theory of atomic collisions* (Springer Science & Business Media)
[35] Gu M F 2004 *Phys. Rev. A* **70** 062704
[36] Norrington P H and Grant I P 1981 *J. Phys. B: Atom. Mol. Phys.* 14 L261
[37] Zatsarinny O, Bartschat K, Fernandez-Menchero L and Tayal S S 2019 *Phys. Rev. A* **99** 023430
[38] Gao X, Han X Y and Li J M 2016 *J. Phys. B: Atom. Mol. Opt. Phys.* **49** 214005
[39] Seaton M J 1983 *Reports on Progress in Physics* **46** 167
[40] Kramida A, Yu Ralchenko, Reader J and NIST ASD Team 2020 *NIST Atomic Spectra Database* (ver. 5.8), [Online]. National Institute of Standards and Technology, Gaithersburg, MD.